Journal of Dynamics, Monitoring and Diagnostics, 2022, 1, 237-250
https://doi.org/10.37965/jdmd.2022.135

ISTP
RESEARCH ARTICLE

CVRgram for Demodulation Band Determination in Bearing Fault Diagnosis under Strong Gear Interference

Pengda Wang,[1] Dezun Zhao,[1] Dongdong Liu,[1] and Lingli Cui[1]
[1]Beijing Key Laboratory of Advanced Manufacturing Technology, Faculty of Materials and Manufacturing, Beijing University of Technology, Beijing 100124

(Received 24 September 2022; Revised 23 December 2022; Accepted 23 December 2022; Published online 23 December 2022)

Abstract: Fault-related resonance frequency band extraction-based demodulation methods are widely used for bearing diagnostics. However, due to the high peaks of strong gear meshing interference, the classical band selection methods have poor performance and cannot work well for bearing fault type detection. As such, the CVRgram-based bearing fault diagnosis method is proposed in this paper. In the proposed method, inspired by the conditional variance (CV) index and root mean square (RMS), a novel index, named the CV/ root mean square (CVR), is first proposed. The CVR index has high robustness for the interference of non-Gaussian or Gaussian noise and has the ability to determine the center frequency of the weak bearing fault-related resonance frequency band under strong interference. Secondly, motived by the Kurtogram, the CVRgram algorithm is developed for adaptively determining the optimal filtering parameters. Finally, the CVRgram-based bearing fault diagnosis method under strong gear meshing interference is proposed. The performance of the CVRgram-based method is verified by both the simulation signal and the experiment signal. The comparison analysis with the Kurtogram, Protrugram, and CVgram-based method shows that the proposed technique has a much better ability for bearing fault detection under strong noise interference.

Keywords: bearing fault diagnosis; CVRgram; gear meshing interference; resonance frequency band detection

I. INTRODUCTION

Bearings are critical components of gearboxes, which are widely used in drive train systems of mechanical equipment. Typical examples include wind turbines, aircraft engines, and helicopter gearboxes [1]. Due to harsh working environments such as shock, heavy load, and high temperature, bearings are easily damaged, and their failure may lead to unplanned shutdowns and increase in maintenance costs or even fatal accidents. In addition, the bearing fault feature is usually submerged in strong interference, such as gear meshing vibration or other background noise [2]. Hence, bearing fault diagnosis under strong gear interference has become an important topic in recent years.

Rolling bearing defects often occur in the loading area; when the rolling elements pass through the defect, a series of impulses are generated, and these impulses will excite high-frequency system resonance. Namely, the vibration signal in the high-frequency resonance band preserves bearing fault information well [3]. Hence, high-frequency resonance extraction is an important step for bearing fault diagnosis.

In the past few decades, a variety of methods have been proposed to select the informative frequency band. Among them, spectral kurtosis is the first systematic indicator. Spectral kurtosis (SK) is defined as the kurtosis of its frequency components and is compared to the variability in the amplitude of the different spectral frequencies [4]. Thus, the SK can be used to indicate the impulsiveness change of a signal with frequency.

Corresponding authors: Lingli Cui (e-mail: acuilingli@163.com); Dezun Zhao (e-mail: dzzhao0903@bjut.edu.cn).

For improving the frequency resolution of the SK, Antoni et al. [5] proposed the Kurtogram, which displays spectral kurtosis values in a visual form on a 2D plane as a function of the central frequency and the bandwidth of the filtered signal.

The Kurtogram is effective to determine optimal filtering parameters; however, its application is limited due to the expensive computation. Then, based on a multi-rate filter bank structure, the Fast Kurtogram was proposed by Antoni [6]. The Fast Kurtogram has a higher calculation efficiency than the Kurtogram; thus, it has been widely used and considered a benchmark technique for mechanical fault diagnosis.

The Kurtogram is constructed based on the kurtosis indicator which is sensitive to impulses; it would fail in cases when the strong non-Gaussian noise contains high peaks than fault impulses. To address this issue, a series of enhanced spectral kurtosis methods were proposed. Firstly, Protrugram was proposed by Tomasz Barszcz et al. [7], and it is based on the kurtosis of the envelope spectrum amplitudes of the narrowband envelope signals calculated in the frequency domain rather than the computation of the kurtosis of the filtered time domain signal. Secondly, Ali Moshrefzadeh and Alessandro Fasana [8] developed the Autogram, which enhances the conventional Kurtogram by computing kurtosis of unbiased autocorrelation of the squared envelope of the demodulated signal. Motivated by ideas in the thermodynamics field, where transients are seen as departures from a state of equilibrium, Jerome Antoni [9] proposed measuring the negentropy of the squared envelope (SE) and the squared envelope spectrum (SES) of the signal. As a result, the SE Infogram and the SES Infogram were defined, respectively. In addition, the Infogram combines the advantages of the Kurtogram's

focus on impulsiveness and the Protrugram's focus on cyclostationarity.

In recent years, some new indicators, such as the Gini index [10], stability index [11], and CV index [12], have been introduced into machinery fault diagnosis due to their high robustness under low SNR or non-Gaussian noise background.

The Gini index was originally introduced in economics and used to measure the income inequality of a nation and was first introduced for the feature extraction of the machinery fault diagnosis in 2017 [10]. Since then, the Gini index is widely applied in this field to solve the gear and bearing fault diagnosis [13,14,15]. The stability index is proposed based on the α-stable distribution, which is an extended form of the classical normal distribution, and it has been successfully used for non-Gaussian noise data pre-processing [11]. The CV index, which is based on a well-known 20-60-20 Rule in the field of management, was used for copper ore crusher-bearing fault diagnosis by Justyna Hebda-Sobkowicz [12] et al. in 2020. In short, the 20-60-20 Rule can be clarified as if a large normal random sample is divided into three sets with different states: one corresponding to the worst (smallest) 20% outcomes, one corresponding to the middle 60% outcomes, and one corresponding to the best (largest) 20% outcomes; then, the variances on appropriate subsets are approximately the same.

The CV index is sensitive to periodic impulses, and it has a good effect on mechanical system fault diagnosis. However, when the measured signal includes multiple vibration components with different amplitudes, the CV index-based method would select the resonance frequency band with a high amplitude, while the resonance frequency band corresponding to a smaller amplitude would be ignored. This phenomenon is very common for gearbox signals, in which relatively weak bearing fault features are often submerged in complex gear vibration [16,17].

As such, inspired by the CV index, a novel index, named CVR, is first proposed in this paper. Since it takes the impulsiveness and energy characteristic of the signal into consideration, the CVR index is sensitive to fault-related impulses with small amplitudes. Secondly, the CVRgram is developed for adaptively determining the optimal filtering parameters. Finally, the CVRgram-based method is proposed for detecting bearing faults under strong gear meshing interference. The proposed method is blind, as it does not require certain knowledge about the target fault.

The remaining parts of this paper are organized as follows: The principle of the CV index is introduced in Section II. In Section III, the novel CVR index and CVRgram are introduced. In Section IV, the proposed CVRgram-based method is presented. In Section V, a simulated faulty bearing signal under strong noise interference is constructed to verify the performance of the proposed method. In Section VI, a faulty bearing signal measured from the gearbox is used to further validate the proposed method. Finally, the Conclusions are drawn in Section VII.

II. REVIEW OF CV INDEX AND MOTIVATION

A. REVIEW OF CV INDEX

The CV is an outstanding index with high robustness under the interference of random impulse noise, and it can be used to distinguish fault-related resonance frequency bands from other frequency bands.

In practical applications, except for the Gaussian noise, other fundamental frequencies may exist in the captured signal obtained from healthy machines. In general, the signal is first decomposed into multiple sub-signals with the application of the frequency band selection method. Since the fault-induced impulses are well preserved in the fault-related-resonance frequency bands, the amplitudes of corresponding sub-signals deviate from normal distribution significantly. While the fundamental frequencies are weakened in other sub-signals, the amplitudes of these sub-signals may not deviate much from the normal distribution. As such, the CV index is effective to locate the resonant frequency band excited by the fault-related periodic impulses.

The details of the CV index are introduced as follows: A set of Gaussian random variables is denoted as $Y \sim N(\mu,\sigma)$, in which μ and σ stand for the mean and standard deviation of the variable, respectively. $\phi_{\mu,\sigma}$ and $\Phi_{\mu,\sigma}$ represent the density function and distribution function of Y, respectively. Let q be the quantile, for any level $0 < q < 0.5$, the left, middle, and right quantile partitioning of Y can be expressed as:

$$\begin{cases} L_q = (-\infty, \Phi^{-1}_{\mu,\sigma}(q)] \\ M_q = (\Phi^{-1}_{\mu,\sigma}(q), \Phi^{-1}_{\mu,\sigma}(1-q)] \\ R_q = (\Phi^{-1}_{\mu,\sigma}(1-q), +\infty] \end{cases} \tag{1}$$

where $\Phi^{-1}_{\mu,\sigma}$ is the inverse of $\Phi_{\mu,\sigma}$, $\Phi^{-1}_{\mu,\sigma}(d)$ represent the d-quantile of Y.

When a set of variables conforms to the normal distribution and the partitioning ratio close to 20%, 60%, and 20%, namely $q \approx 0.2$, the conditional variances of each subset are equal, and the following equation can be obtained,

$$\sigma^2_{L_q} = \sigma^2_{M_q} = \sigma^2_{R_q} \tag{2}$$

where L_q, M_q, and R_q represent the subsets of the sample, $\sigma^2_{L_q}$, $\sigma^2_{M_q}$, and $\sigma^2_{R_q}$ represent the conditional variance of subsets L_q, M_q, and R_q, respectively.

It should be noted that the 20%-60%-20% ratio is the unique quantile (three sets) partitioning satisfying Eq. (2), corresponding partitioning is presented in Fig. 1(a).

In short, Eq. (2) can be described as follows: when a large normal random sample is divided into three sets with different states, one corresponding to the worst (smallest) 20% outcomes, one corresponding to the middle 60% outcomes, and one corresponding to the best (largest) 20% outcomes; as a result, the conditional variances of the three sets roughly equal to each other.

Since the unique ratio satisfying Eq. (2) is equal to 20%, 60%, and 20%, this property can be used to construct a statistic. A statistical framework introduced in [18] was briefly summarized, namely for a given random sample $(Y_1, Y_2, \ldots, Y_n)$ from Y, a test statistic N is constructed as follows,

$$N = \frac{1}{\rho}\left(\frac{\sigma^2_{L_q} - \sigma^2_{M_q}}{\sigma^2} + \frac{\sigma^2_{R_q} - \sigma^2_{M_q}}{\sigma^2}\right) * \sqrt{n} \tag{3}$$

where q=0.2; $\rho \in R$ is a constant; σ^2 is the sample variance; and σ^2_A is set A conditional sample variance.

Eq. (3) could be described as: by comparing the conditional variances with the conditional central variance,

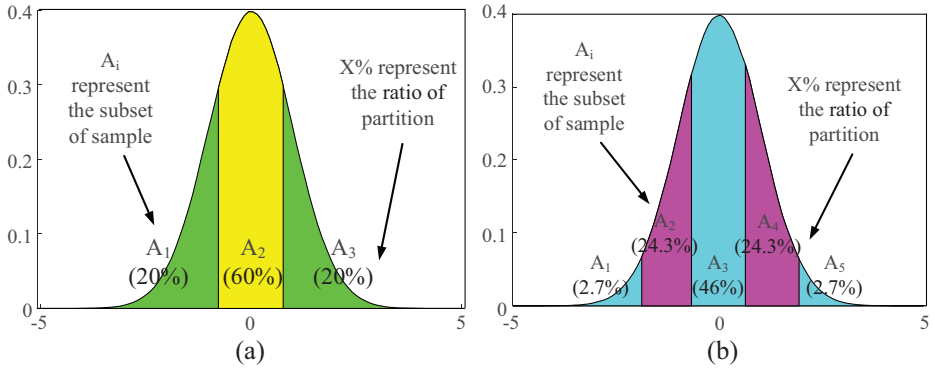

Fig. 1. Density function of the standard normal distribution with different quantiles.

it can be verified whether the sample comes from Gaussian distribution. If the sample coincides with normal distribution, the value of N should be approximately equal to 0 [18]. When the sample $(Y_1,Y_2,\ldots,Y_n)$ comes from heavy-tailed distribution, the statistic N achieves a positive value due to high values of conditional tail variances on sets L_q and R_q. In general, the statistic N could be regarded as the measure of tail fatness, namely the fatter the tails, the bigger the value of N.

It is relatively easy to calculate the value of N for a given sample. For example, the steps to calculate $\sigma^2_{L_q}$ can be described as follows: (a) order the sample; (b) subsample the first [q × n] observations; (c) calculate the standard sample variance for the subsample.

B. MOTIVATION FOR APPLICATION OF CV INDEX

Since the CV index has high robustness under non-Gaussian noise, the CV-based method has been successfully applied to copper ore crushers in the mining industry [12].

However, when vibration signals include multiple vibration components, the resonance frequency band, whose amplitude is dominant, can be captured by the CV index. In other words, CV index cannot work well for detecting the relatively weak bearing fault-related frequency bands when strong interference exists. For example, when the gearbox bearing has a local fault, its resonance frequency amplitudes are relatively weak compared with the gear meshing harmonics, and the CV-based method only locates gear meshing harmonic related frequency band, while the frequency band associated with bearing faults is submerged.

III. CVRgram

A. THEORY OF CVR INDEX

For improving the CV index, the CVR index is defined by introducing the RMS. The CVR index inherits the advantages of high robustness of the CV index to non-Gaussian noise and can highlight the resonance frequency band excited by bearings under strong harmonics interference. The details of the CVR index are introduced as follows.

According to [19] Remark 3, the Gaussian population could be divided into three, five, and seven sets with certain quantiles for creating a dispersion balance.

The data are divided into 5 groups in this paper to calculate the CV index. For five quantile conditioning subsets, the unique set of quantiles guaranteeing conditional variance equality is 0.027/0.243/0.460/0.243/0.027. The partitioning is as follows,

$$\begin{cases} A_1 = (-\infty,\Phi^{-1}_{\mu,\sigma}(0.027)] \\ A_2 = (\Phi^{-1}_{\mu,\sigma}(0.027),\Phi^{-1}_{\mu,\sigma}(0.270)] \\ A_3 = (\Phi^{-1}_{\mu,\sigma}(0.270),\Phi^{-1}_{\mu,\sigma}(0.730)] \\ A_4 = (\Phi^{-1}_{\mu,\sigma}(0.730),\Phi^{-1}_{\mu,\sigma}(0.973)] \\ A_5 = (\Phi^{-1}_{\mu,\sigma}(0.973),+\infty] \end{cases} \tag{4}$$

Then, the following equation can be obtained,

$$\sigma^2_{A_1} = \sigma^2_{A_2} = \sigma^2_{A_3} = \sigma^2_{A_4} = \sigma^2_{A_5} \tag{5}$$

When Eq. (5) is satisfied, a balanced distribution for the conditional population is achieved. The graphical illustration of the five partitioning is presented in Fig. 1(b).

For reducing the strong non-Gaussian noise, three subsets are used to construct an indicator. In this case, the rest of the sets which might relate to non-Gaussian components with high amplitudes are not taken into consideration.

For the samples $(Y_1,Y_2,\ldots,Y_n)$, a statistic that takes sample conditional variances on sets A_2, A_3, and A_4 into account is constructed as,

$$N5 = \left(\frac{\sigma^2_{A_2} - \sigma^2_{A_3}}{\sigma^2} + \frac{\sigma^2_{A_4} - \sigma^2_{A_3}}{\sigma^2}\right) * \sqrt{n} \tag{6}$$

where $\sigma^2$is the sample variance, and σ^2_A is the conditional sample variance of set A.

The statistic $N5$ could be used to measure the degree that the sample deviates from the normal distribution. Namely, the informative frequency band can be located by statistic $N5$. However, based on statistic $N5$, only the frequency band with dominant amplitude can be obtained, and the weak resonance frequency excited by bearing would be ignored. As such, an energy factor, which is RMS, is introduced into the CV index.

For the signal $x(t)$, its RMS is defined as,

$$RMS(x(t)) = \langle |x(t)|^2 \rangle^{\frac{1}{2}} \tag{7}$$

For improving stability, the Hilbert envelope is applied to the signal to eliminate distractions. As a result, the shape of fault-relating impulses becomes clearer. The envelope signal is calculated as [20]

$$x_h(t) = Hilbert(x(t)) = \frac{1}{\pi}\int_{-\infty}^{+\infty} \frac{x(\tau)}{t-\tau} d\tau \tag{8}$$

where $x_{he}(t)$ represents the Hilbert envelope of signal$x(t)$.

$$x_a(t) = abs(x_h(t)) \tag{9}$$

where $abs(\cdot)$ is used to calculate the module, $x_a(t)$ represents the amplitude signal of $x_h(t)$.

Based on the above envelope process, a series of extreme values can be obtained. Then, the RMS of extreme values instead of all the data is calculated to describe the energy characteristic of the signal. The RMS of the extreme values is calculated as follows,

$$RMS_{ev} = RMS(findpeaks(x_a(t))) \tag{10}$$

where $findpeaks(\cdot)$ is the function for finding the same number of extreme values of the envelope curve of sub-signals, RMS_{ev} represents the RMS of the selected extreme values. The process of obtaining the extreme values for calculating the RMS is shown in Fig. 2.

Hence, the CVR index is constructed as,

$$CVR(x(t)) = \frac{1}{RMS_{ev}} * N5(x(t)) \tag{11}$$

Based on the above analysis, a new CVR index is constructed, in which the RMS_{ev} acts as an energy factor, and the index is sensitive to the energy characteristic and periodicity of the signal. The CVR index can be used to locate the bearing fault-related resonance frequency band under strong interference.

Similarly to what has been proposed in [21], a hypothesis test is defined as follows:

H_0:"The vibration signal does not contain a fault at the frequency fcf_0"

H_1:"The vibration signal contains a fault at the frequency fcf_0"

where fcf_0 represents the fault characteristic frequency.

Reject the null hypothesis H_0 if "The vibration signal contains a fault at the frequency fcf_0 if relatively prominent peaks can be found at the frequency fcf_0 and its harmonics on the envelope spectrum."

In this paper, the proposed CVRgram-based method aims to make the FCF and its harmonics-related spectral lines more obvious on the envelope spectrum. Since the proposed method cannot be quantified, there is no fixed threshold, and the diagnosis depends on experience.

B. CVR_{gram} CALCULATION

Based on the CVR index, the CVRgram is constructed in this subsection. The principle of the CVRgram is to search

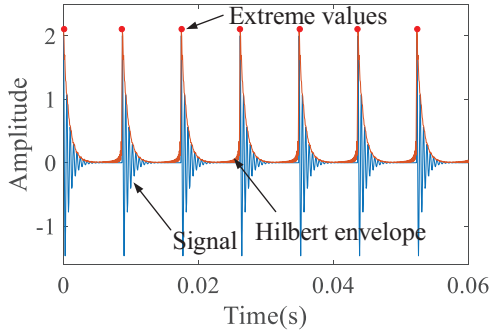

Fig. 2. The diagram of extremal value solution.

for the optimal center frequency/bandwidth parameters in the entire frequency band plane for locating the bearing fault-related resonance frequency bands. The main steps for constructing the CVRgram are as follows.

(a) Let $h(n)$ be a low-pass prototype filter with a cut-off frequency $f_c = \frac{1}{8} + \varepsilon, \varepsilon \geq 0$. The normalized frequency is adopted here, namely the sampling frequency is 1. Then, two quasi-analytic low-pass and high-pass analysis filters $h_0(n)$ and $h_1(n)$ from $h(n)$ are constructed, in the frequency bands [0,1/4] and [1/4,1/2], respectively:

$$\begin{aligned} h_0(n) &= h(n)e^{\frac{j\pi n}{4}} \\ &= h(n)[\cos\left(\frac{\pi n}{4}\right) + j\,\sin\left(\frac{\pi n}{4}\right) \end{aligned} \tag{12}$$

$$\begin{aligned} h_1(n) &= h(n)e^{\frac{j3\pi n}{4}} \\ &= h(n)[\cos\left(\frac{3\pi n}{4}\right) + j\,\sin\left(\frac{3\pi n}{4}\right) \end{aligned} \tag{13}$$

Let filters $h_0(n)$ and $h_1(n)$ perform the elementary low-pass and high-pass decomposition, with band-pass ranges [0,1/4] and [1/4,1/2], respectively. $c_k^i(n)$is used to represent the sequence of coefficients issued from the ith filter with $i = 0,1,2,\ldots,2^k - 1$, at the kth level in the decomposition tree, $k = 0,1,2,\ldots$, after filtration with $h_0(n)$ and $h_1(n)$ and down-sampling by factor 2, this sequence offsprings two new sequences $c_{k+1}^{2i}(n)$ and $c_{k+1}^{2i+1}(n)$ at level k+1. At each level, the number of filtered sequences is increased by a factor of 2, but their respective length is also decreased by the same factor so that overall the total amount of data remains the same. The recursive algorithm of the dual-sub-band decomposition is as follows,

$$c_{k+1}^{2i}(n) = h_0(m) * c_k^i \tag{14}$$

$$c_{k+1}^{2i+1}(n) = h_1(m) * c_k^i \tag{15}$$

where * represents convolution, k is the decomposition level (k = 0, 1, ...), i is the coefficient sequence of filter (i = 0, ...,2k−1).

The coefficients $c_k^i(n)$ can be interpreted as the complex envelope of signal $x(n)$ positioned on the central frequency,

$$f_i = \frac{2i+1}{2^{-k-2}} \tag{16}$$

and with bandwidth (frequency resolution),

$$\Delta f_k = 2^{-k-1} \tag{17}$$

Based on the above algorithm, tree filter banks are generated, which sample the (frequency/frequency resolution) plane through a dyadic grid. However, this sampling is too coarse in some applications where the narrowband transients need to be detected. Hence, a three-sub-band decomposition method is integrated on the basis of the dual-sub-band decomposition with negligible extra computing cost [6].

The principle of the three-sub-band decomposition is similar to that of the dual-sub-band decomposition. By designing three quasi-analytical band-pass filters $g_0(n)$, $g_1(n)$, $g_2(n)$, the band-pass ranges [0,1/6], [1/6,1/3], and [1/3,1/2] are obtained, respectively. Finally, the three-sub-band decomposition result is inserted into the two-sub-band

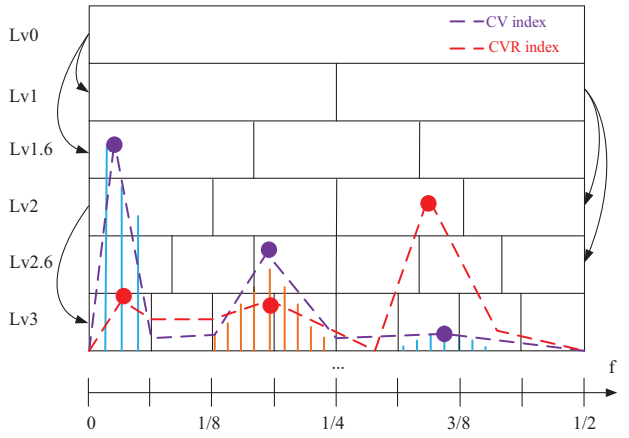

Fig. 3. Paving of the (frequency/ frequency resolution) plane in case of a 1/3-binary tree.

ones based on the number sorted by sub-bands at each level (from least to most), as illustrated in Fig. 3. To satisfy the sampling theory, Lv0 range from 0 to 1/2×sampling frequency, Lv1, Lv2, Lv3, . . . divide Lv0 into two, four, eight, . . . equal parts, respectively. Similarly, Lv1.6, Lv2.6, and Lv3.6 . . . divide Lv0 into three, six, twelve, . . . equal parts, respectively.

(b) Calculate the CVR value of each sub-band signal. The CVR value of each sub-band signal at the center frequency f_i and the bandwidth Δf_k can be calculated as

$$CVR(f_i,\Delta f_k) = \frac{CV(f_i,\Delta f_k)}{RMS_{ev}(f_i,\Delta f_k)} \tag{18}$$

(c) Find the frequency band with the largest CVR value on the CVRgram. The parameters of this frequency band correspond to the target center frequency and bandwidth parameters. The band-pass filter designed with this parameter can be used to extract bearing fault-related resonance frequency bands under strong interference. The schematic diagram of the CV and CVR index is presented in Fig. 3. When the gearbox bearing has a local fault, the CV value is the largest in the gear-related frequency band, while the largest CVR index value is acquired in the bearing fault-related resonance frequency band. Namely, under the strong gear meshing interference, the CV-based method would select a gear meshing-related frequency band, while the CVRgram-based method can effectively locate the bearing fault-related resonance frequency band.

(d) CVRgram decomposition guideline in a certain range. The higher the degree of band refinement, the more accurate the filtering parameters obtained; however, when exceeding a certain limit, with the increase of filter bank level, the bandwidth of the higher level becomes too narrow, resulting in insufficient fault information in the sub-band. Therefore, too many levels of filter banks would lead to a waste of computing resources, and it is necessary to set a threshold for calculating the levels of filter banks in the CVRgram.

Through experimental comparison, it is concluded that when the bandwidth of the filter is 3-5 times bigger than the fault characteristic frequency (FCF), the filtered signal contains enough fault features [7].

Based on the above analysis, the CVRgram decomposition guideline is shown as,

$$f_{bmin} \approx C \cdot f_r \cdot FCC_i = C \cdot f_r \cdot \frac{D}{d}\left[1 - \left(\frac{d}{D}\right)^2 cos^2\alpha\right] \tag{19}$$

where f_{bmin} represents the minimum bandwidth of the filter, $C \in [3,5]$denotes a constant, f_r represents the rotational frequency of bearing, and FCC_i is the fault characteristic coefficient (FCC) of the ball, D is the pitch diameter of the bearing, d is the diameter of the rolling elements, α is the contact angle of the bearing. In engineering applications, the rotational frequency of the gearbox is easy to obtain, namely bearing rotational frequency f_r can be determined. In addition, the FCC of the ball FCC_i is the smallest among bearing FCCs, and the corresponding minimum bandwidth of the filter is suitable for bearing other fault types. Therefore, we can estimate the minimum bandwidth to determine the number of decomposition layers of the tree filter bank.

IV. CVRgram-BASED BEARING FAULT DIAGNOSIS METHOD

For effectively detecting bearing fault type under strong gear meshing interference, the CVRgram-related bearing fault diagnosis method is proposed in this section. The flow chart of the CVRgram-based bearing fault diagnosis method is shown in Fig. 4, and its main steps are shown as follows.

(a) Process the bearing vibration signal using the CVRgram. As a result, the optimal filtering parameters are obtained.

(b) Design an optimal filter based on the optimal filtering parameters, and the filtered signal, which includes abundant bearing fault information, is obtained.

(c) Calculate the envelope spectrum of the filtered signal. In the envelope spectrum, the spectral lines related to the bearing fault are dominant.

(d) Detect bearing fault type based on the envelope spectrum and bearing FCF, which are calculated using the rotating frequency and fault characteristic coefficient.

The main contributions of this paper are as follows: (i) The CVR index is proposed, and it can be used to extract weak bearing fault-related features under strong meshing

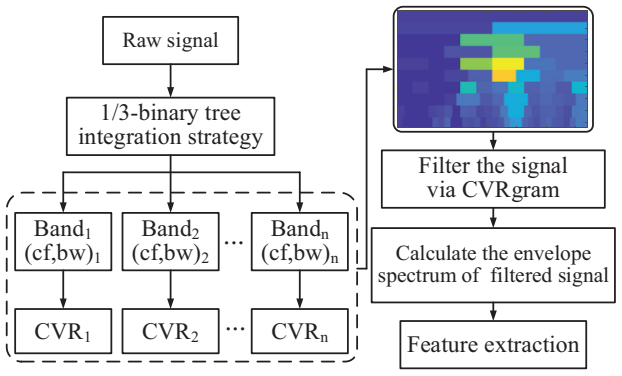

Fig. 4. Schematic description of the CVRgram procedure.

interference and has high robustness under the interference of the random impulse noise. (ii) Based on the CVR index, a CVRgram-based bearing fault diagnosis method is developed, and the method can be used to adaptively determine the optimal filtering parameters under strong interference.

V. SIMULATION ANALYSIS

In this section, the simulation signal of fault bearing with a constant rotating speed under strong gear meshing interference is constructed for verifying the effectiveness of the proposed method. Furthermore, the Kurtogram and CVgram-based methods are used as a comparison to highlight the performance of the CVRgram-based method. This section contains two parts: A. simulation signal is constructed and the effectiveness of the CVR-based method is verified, and B. comparison analysis is presented.

A. SIMULATION MODEL AND ANALYSIS RESULTS

In this subsection, a simulation model, which represents the vibration coming from an outer race fault bearing in a gearbox, is presented. The simulation model contains three main components: the sine harmonics ($S_{gear}(t)$) generated by gear meshing, the cyclic impulses ($S_{bearing}(t)$) related to the bearing local damage, and the white Gaussian noise ($n(t)$). The mathematical expressions are shown in Eqs. (20)-(22).

$$S(t) = S_{bearing}(t) + S_{gear}(t) + n(\mathrm{t}) \tag{20}$$

where $S(t)$ is the integrated simulation signal, $S_{gear}(t)$ and $S_{bearing}(t)$ represent components related to gear meshing and fault bearing respectively, $n(t)$ is the Gaussian noise.

The vibration signal model of healthy gear is calculated as [22]

$$S_{gear}(t) = \sum_{m=0}^{M} A_m \cos(2\pi m f_m(t) + \phi_m) \tag{21}$$

where A_m represent the amplitude of meshing harmonics, and there were set to 40,30, and 20, respectively. f_m is the meshing frequency of the gear, and it is 244 Hz in this paper. ϕ_m represents the initial phase angle of the gear and is set to 0.

The vibration signal model of fault bearing is defined as [23]

$$S_{bearing}(t) = \sum_{i=1}^{N} A_o * e^{-\beta(t-iT-\tau_i)} * \cos(2\pi f_c(t-iT-\tau_i) + \phi_\omega) * u(t-iT-\tau_i) \tag{22}$$

where β and τ_i represent the attenuation coefficient and slip coefficient of the rolling element, respectively. For simplification, we set β=1200 and $\tau_i = 0.01$. ϕ_ω is set to 0, which represents the initial phase angle of the bearing. A_o and T represent the amplitude and period of the periodic impulses caused by bearing fault, respectively. f_c is the frequency of the bearing fault-related resonance, which is only related to the bearing.

In this paper, the length of the simulated signal is 3 s and the sampling frequency is 24,000 Hz, and relevant parameters are listed in Table I. The time domain waveform of the simulated signal and corresponding envelope spectrum are shown in Fig. 5(a) and (b), respectively. In Fig. 5(b), the prominent peaks can be found at 246 Hz and 492 Hz, which are gear meshing frequency and its harmonics, and the bearing FCF cannot be identified.

The simulated signal is processed using the CVRgram-based method, and the results are shown in Fig. 6. The CVRgram of the simulated signal is presented in Fig. 6(a), from which a band with the center frequency of 8250 Hz and the bandwidth of 1500 Hz is selected. Based on the optimal filtering parameters determined by CVRgram, the band-pass filtering algorithm is applied to the simulated signal. Then, the envelope spectrum of the filtered signal is calculated, as shown in Fig. 6(b), from which it can be found that the spectral lines representing the outer race FCF (40 Hz) and its harmonics can be identified.

Table I. Parameters of the simulation model

Meaning	Value
Sampling frequency, F_s	24,000 Hz
Center frequency, f_c	8000 Hz
FCF of the outer race	40 Hz
The amplitude of impulses, A_o	15
Rotational frequency, f_r	11.2 Hz
Number of gear teeth, Z	22
Meshing frequency, f_m	246.4 Hz
The amplitude of meshing harmonics, A_m	40/30/20
SNR	−10 dB

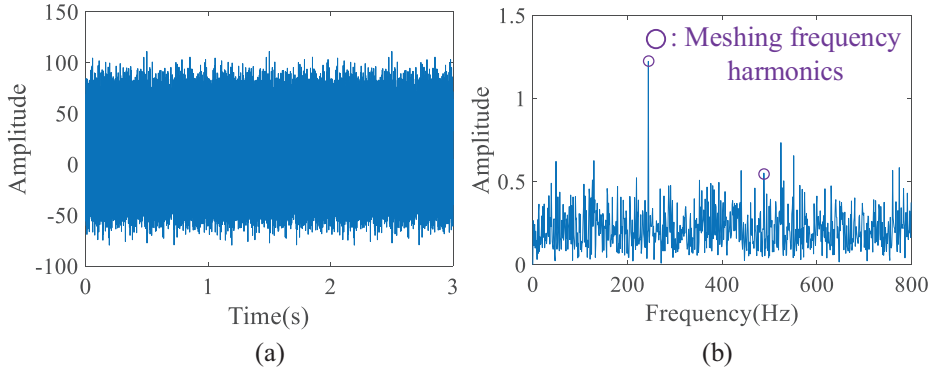

Fig. 5. Simulated signal. (a) Time domain waveform, (b) Envelope spectrum.

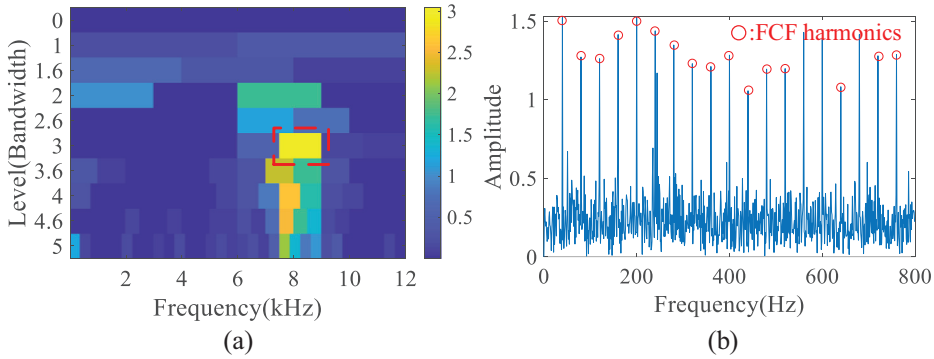

Fig. 6. Analysis results using the CVRgram-based method. (a) CVRgram, (b) Envelope spectrum of the filtered signal.

It can be concluded that the CVRgram-based method is effective to locate the bearing fault-related frequency band under strong gear meshing interference.

B. COMPARISON ANALYSIS

The Kurtogram has been widely used in bearing fault diagnosis, and the CVgram-based method has been used in bearing fault diagnosis with high robustness under non-Gaussian noise. Hence, the above two methods are used to verify the superiority of the CVRgram-based method in this subsection.

Firstly, the CVgram analysis results are shown in Fig. 7. The CVgram is presented in Fig. 7(a), from which the maximum CV value corresponds to the frequency band with a center frequency of 750 Hz and a bandwidth of 1500 Hz. The envelope spectrum of the filtered signal is displayed in Fig. 7(b), in which only gear meshing frequency-related spectral lines can be identified.

Based on the above analysis, when the signal contains gear meshing components with high energy and bearing fault impulsive components with relatively weak energy, the CVgram-based method cannot work well for bearing fault feature extraction.

Similar to the CVgram-based method, a low-frequency band that contains gear meshing frequency is located by the Kurtogram. The Kurtogram is presented in Fig. 8(a), in which a frequency band with a center frequency of 2 k Hz and a bandwidth of 4 k Hz has the maximum kurtosis. Based on the optimal filtering parameters determined by the Kurtogram, a band-pass filter is designed to process the signal, and the envelope spectrum of the filtered signal is

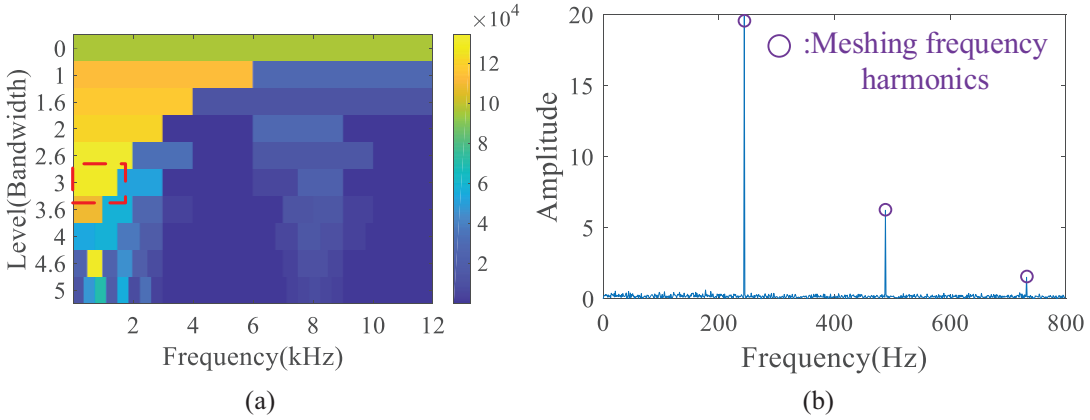

Fig. 7. Analysis results using the CVgram-based method. (a) CVgram, (b) Envelope spectrum of the filtered signal.

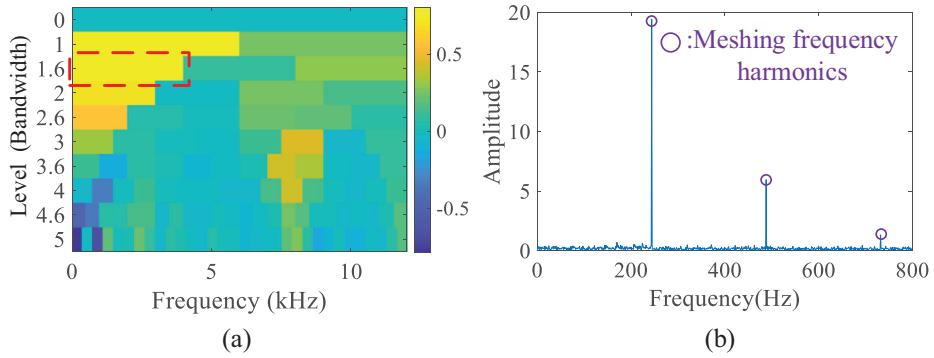

Fig. 8. Analysis results using the Kurtogram-based method. (a) Kurtogram, (b) Envelope spectrum of the filtered signal.

shown in Fig. 8(b). From the envelope spectrum, only gear meshing harmonics can be captured.

When processing gearbox bearing fault signal, the demodulation band obtained by the Kurtogram and CVgram algorithm are related to the gear meshing, while the CVRgram would locate the resonance frequency band excited by bearing fault. Hence, the proposed method has a much better ability to detect bearing faults under gear meshing interference.

To further quantify the robustness of the proposed method against the gear mesh interference under different signal-to-noise ratios, three cases with different amplitudes of gear meshing frequency are built to simulate the different SNR circumstances.

Then, a novel indicator named amplitude of envelope spectrum ratio (AESR) is constructed based on the theory that the better the filtering result, the clearer the FCF in the envelope spectrum. Here, three cases with different amplitudes of gear meshing frequency are built to simulate the different SNR circumstances. Hence, the ratio of the amplitudes of the FCF to the sum of the amplitudes of all other components in the envelope spectrum can be used to evaluate the superiority of the methods. Namely, the higher value of the AESR, the much better performance of the method. The AESR is defined as,

$$AESR = \frac{\sum_1^M AFCF}{\sum AES} \tag{23}$$

where $M \leq 3$, $AFCF$ denotes the amplitudes of the FCF, and AES is the amplitudes of all other components in the envelope spectrum.

The AESR indicator of the envelope spectra under different amplitudes of gear meshing frequency is shown in Table II. The AESR is calculated by the CVRgram, CVgram, Kurtogram, and Protrugram-based methods, respectively, as shown in Fig. 9, from which it is found that the CVRgram-based method has the biggest AESR value. It means the filtering effect achieved by the proposed method is the best.

Table II. Amplitudes of gear meshing and bearing fault

Component	Case 1	Case 2	Case 3
Amplitude of meshing frequency	50,40,30	40,30,20	30,20,10
Amplitude of bearing FCF	15	15	15

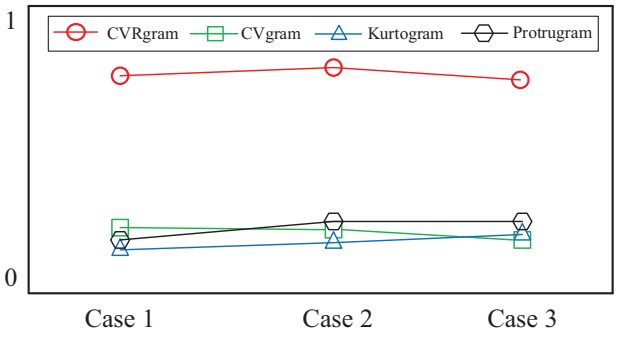

Fig. 9. AESR values calculated by CVRgram, CVgram, Kurtogram, and Protrugram-based methods under different cases

VI. EXPERIMENTAL ANALYSIS

The effectiveness of the CVRgram-based method for bearing fault feature extraction under strong gear meshing interference is further validated using the experiment signal, which is captured from the gearbox test bench at Soochow University. The experiment setup is shown in Fig. 10. A through crack fault with a width of 0.4 mm was cut on the bearing outer race to simulate a local defect, and the installation position of the faulty bearing is shown in Fig. 10. The power generated by the DC motor passes through a gearbox and a set of supporting bearings and finally arrives the experimental gearbox. To reduce the influence of the transmission path, an acceleration sensor is mounted on top of the faulty bearing to measure its vibration signal. The data acquisition system mainly consisted of a signal acquisition instrument with model INV3018C and a computer. The model of the experimental bearings is 30206, and the detailed parameters of the faulty bearing and gearbox are listed in Tables III and IV, respectively. The motor speed is 1480 r/min, and the sampling frequency is 25.6 kHz.

The FCF of the outer race and inner race of the bearing is shown in Eq (24) and Eq (25), respectively,

$$FCF_O = FCC_o * f_r = \frac{z}{2}\left[1 - \frac{d}{D}cos\alpha\right] \tag{24}$$

$$FCF_i = FCC_i * f_r = \frac{z}{2}\left[1 + \frac{d}{D}cos\alpha\right] \tag{25}$$

where f_r is the rotation frequency of the driving shaft, D is the pitch diameter of the bearing, d is the diameter of the rolling elements, α is the contact angle of the bearing, and the number of rolling elements is z. FCC_o and FCC_i are FCCs of the outer race and inner race, respectively. It is assumed that there is no sliding between the rolling elements and the inner and outer rings.

Based on Eqs. (24) and (25), the FCF of the bearing outer race and inner race in this experiment is calculated as 174.3 Hz and 213.4 Hz.

To verify the effectiveness of the proposed method, two types of fault cases are separately carried out. One case is that the localized fault appears in the outer race of the rolling bearing, and another is that the localized fault appears in the inner race. In both cases, the duration of the signal is 2.5 s.

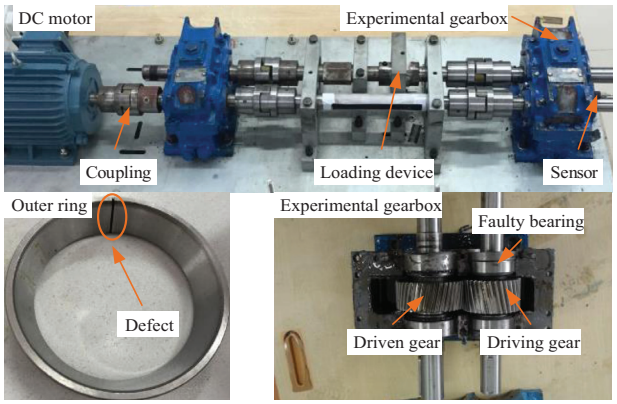

Fig. 10. Experiment setup.

Table III. Test gear parameters

Parameters	Number of teeth	Rotation frequency *fs* (Hz)	Rotation period T_s (s)	Meshing frequency f_c (Hz)
Driving gear	34	24.67	0.041	839
Driven gear	42	19.98	0.05	

Table IV. Test bearing parameters

Inner diameter *d* (mm)	Outer diameter *D* (mm)	Diameter of rolling element d_0 (mm)	Number of rolling element	Contact angle (°)
30	62	8	17	14.036

A. ROLLING BEARING WITH OUTER RACE FAULT

In this case, the proposed method is testified using the vibration data generated by bearing outer race fault, and the CVgram, Kurtogram, and Protrugram-based methods are used for comparison.

The time domain waveform of the vibration signal and corresponding envelope spectrum is presented in Fig. 11(a) and (b), respectively. It can be seen that the rotational frequency and its harmonics-related spectral lines are dominant, and the bearing FCF is submerged.

Fig. 11(c) shows the CVRgram, from which it is found that the maximum CVR value corresponds to the center frequency of 7466 Hz with a bandwidth of 2133 Hz. Based on the optimal filtering parameters determined by the CVRgram, a band-pass filtering algorithm is applied to the vibration signal. The envelope spectrum of the filtered signal is shown in Fig. 11(d), it is obvious that the spectral lines representing the FCF of the outer race (174.3 Hz) and its harmonics are dominant, and there are no other interference components.

For comparison, the CVgram, Kurtogram, and Protrugram are used to process the vibration data.

Firstly, the CVgram is presented in Fig. 12(a), in which the maximum CV value corresponds to the center frequency of 5133 Hz with a bandwidth of 2133 Hz. According to the band selection result, an optimal filter is designed to process the signal. Fig. 12(b) shows the envelope spectrum of the filtered signal, in which spectral lines representing the rotational frequency of the drive shaft and the driven shaft and their harmonics are dominant, while the bearing outer race FCF (174.3 Hz) and its harmonics are submerged in interference components.

Then, the vibration signal is processed by the Kurtogram-based method, and the results are shown in Fig. 13. The Kurtogram is displayed in Fig. 13(a), from which the maximum kurtosis value corresponds to the ending of the frequency band. Based on the optimal filtering parameters determined by Kurtogram, a band-pass filtering algorithm is

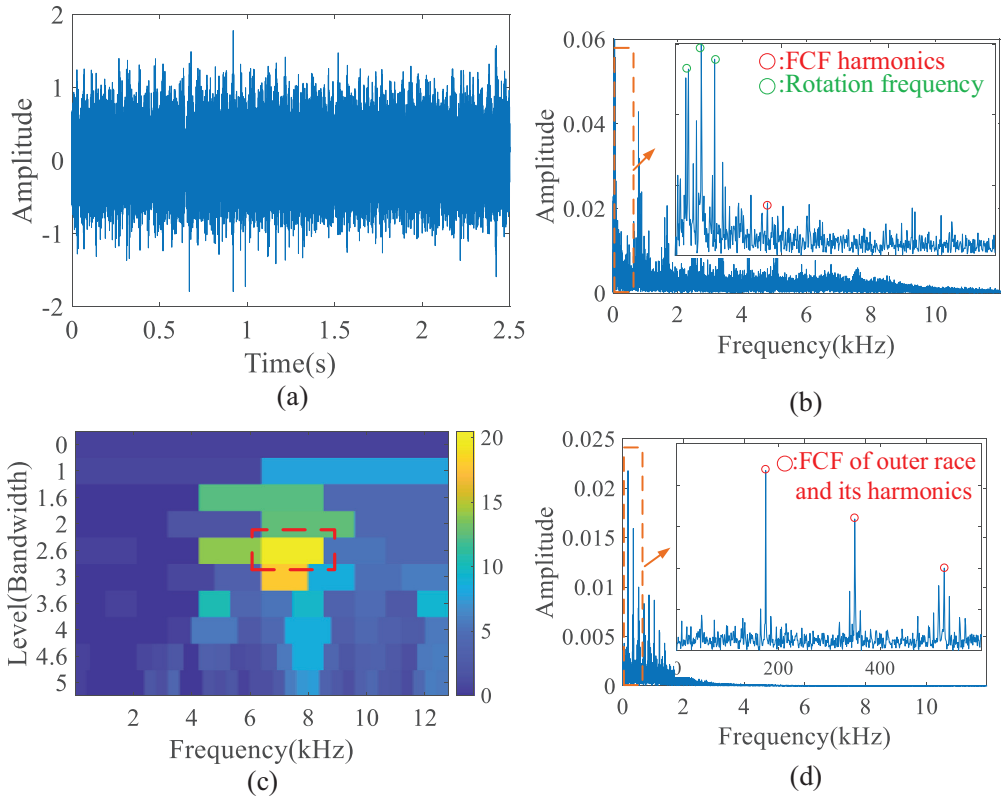

Fig. 11. CVRgram results of vibration data of bearing with outer race fault. (a) Raw vibration signal, (b) Envelope spectrum of the raw signal, (c) CVRgram of the raw signal, and (d) Envelope spectrum of the filtered signal.

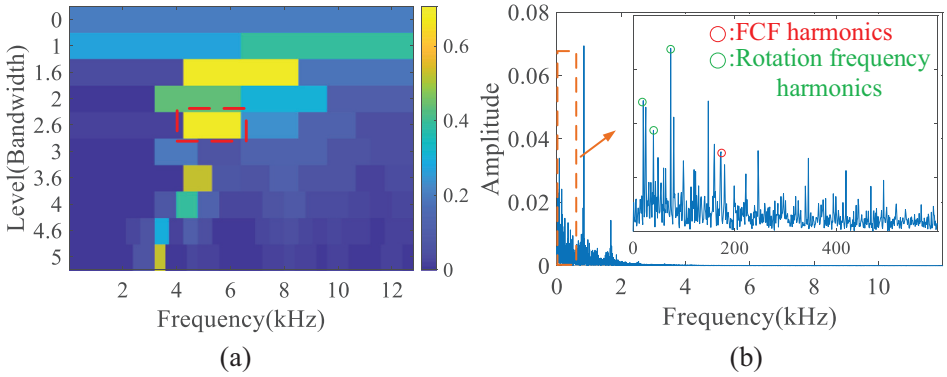

Fig. 12. Analysis results of outer race fault signal using CVgram-based method. (a) CVgram and (b) Envelope spectrum of the filtered signal.

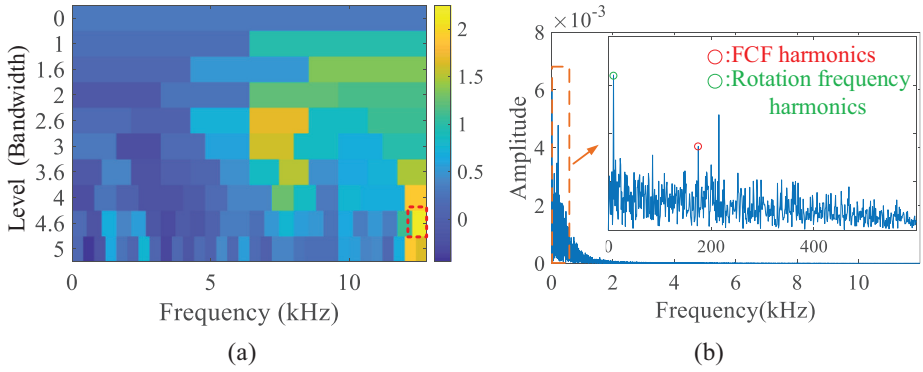

Fig. 13. Analysis results of outer race fault signal using Kurtogram-based method. (a) Kurtogram and (b) Envelope spectrum of the filtered signal.

applied to the signal. Fig. 13(b) is the envelope spectrum of the filtered signal, in which we can observe that spectral lines representing the FCF of the outer race (174.3 Hz) and its harmonics are buried in noise.

Finally, based on the Protrugram as shown in Fig. 14(a), the central frequency and the bandwidth of the filter are 12267 Hz and 1066 Hz, and the target level is 3.6. The envelope spectrum of the filtered signal is shown in Fig. 14(b). It can be found that the rotational frequency harmonics-related spectral lines are more dominant than the bearing fault-related spectral lines.

In summary, when processing signals of gearbox bearing with outer race fault, the Kurtogram, and Protrugram-based methods cannot work well. For the CVgram-based method, due to the CV index having strong robustness against the noise, the CVgram would locate a frequency band containing more gear information. Different from comparison methods, the CVRgram can select the bearing outer race fault-related frequency band. Hence, the proposed method has a much better ability to detect bearing outer race fault under gear meshing interference compared with the CVgram, Kurtogram, and Protrugram.

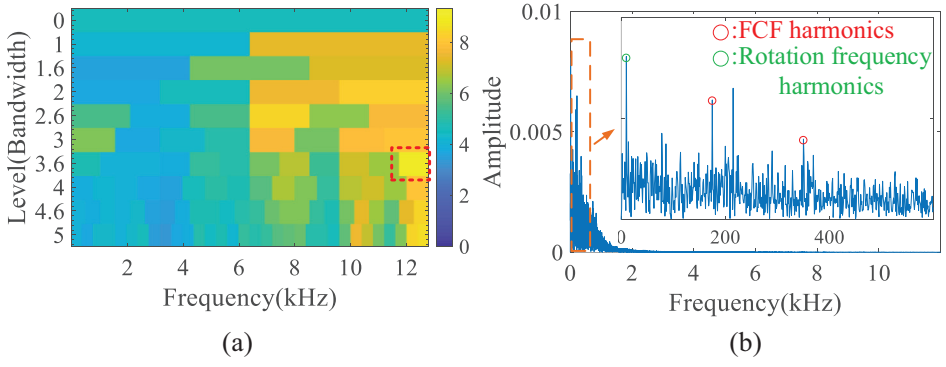

Fig. 14. Analysis results of outer race fault signal using Protrugram-based method. (a) Protrugram and (b) Envelope spectrum of the filtered signal.

B. ROLLING BEARING WITH INNER RACE FAULT

In this case, the CVRgram-based method is verified using the vibration signal generated by the bearing inner race fault. The comparative analysis with the CVgram-based method, Kurtogram-based method, and Protrugram-based method is also discussed.

The time domain waveform of the bearing vibration signal with inner race fault and its envelope spectrum is displayed in Fig. 15(a) and (b), respectively. In Fig. 15(b), the FCF of the inner race (213.4 Hz) is buried in strong noise, and bearing fault cannot be detected.

Then, the measured signal is processed by the CVRgram, and the result is shown in Fig. 15(c). Based on the CVRgram, it can be obtained that the target level is 3.6, the central frequency is 8000 Hz, and the bandwidth is 1067 Hz. Based on the filtering parameters determined by CVRgram, the filtered signal is obtained, and its envelope spectrum is shown in Fig. 15(d), in which the inner race fault-related spectral peak can be recognized. Hence, we can conclude that the developed technique is effective to detect bearing inner race faults.

For comparison, the bearing vibration signal with inner race fault is processed using the CVgram, Kurtogram, and Protrugram, respectively.

Firstly, the demodulation band selected by the CVgram algorithm is shown in Fig. 16(a), and the corresponding envelope spectrum is shown in Fig. 16(b). It can be seen that the inner race FCF-related spectral line is submerged in

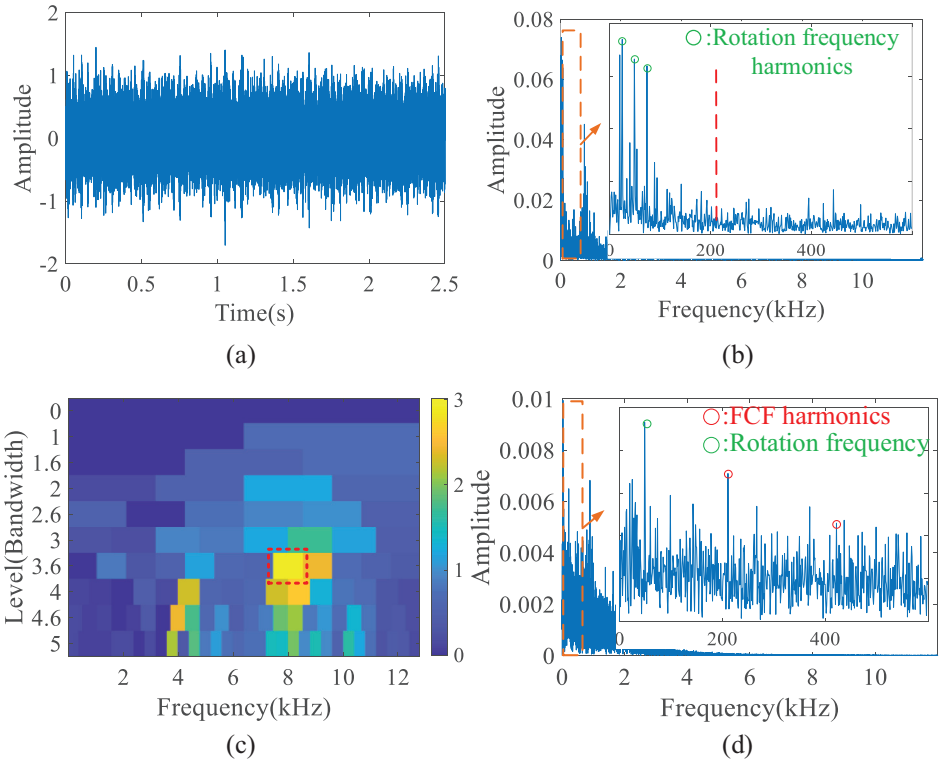

Fig. 15. CVRgram results of vibration data of bearing with inner race fault. (a) Raw vibration signal, (b) Envelope spectrum of the raw signal, (c) CVRgram of the raw signal, and (d) Envelope spectrum of the filtered signal.

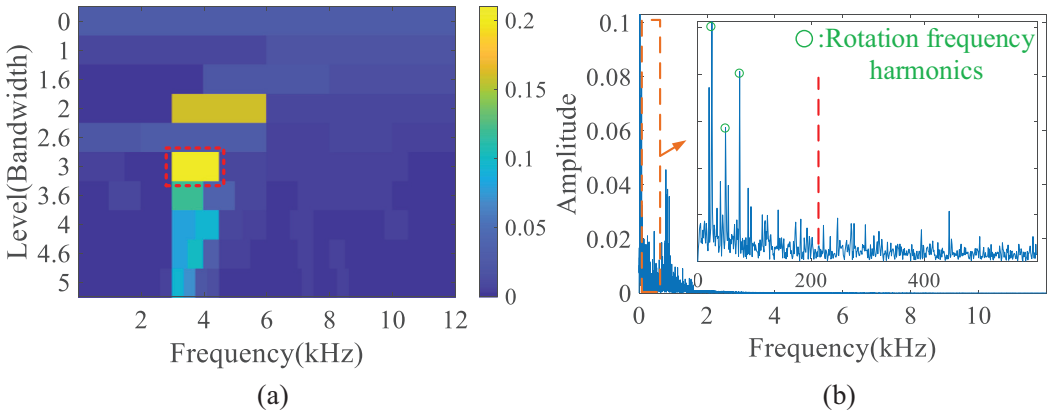

Fig. 16. Analysis results of inner race fault signal using CVgram-based method. (a) CVgram and (b) Envelope spectrum of the filtered signal.

background noise, and it is difficult to detect the bearing inner race fault.

Secondly, the bearing signal is processed by the Kurtogram algorithm, and the results are displayed in Fig. 17. A frequency band (around 4000 Hz) is located as shown in Fig. 17(a), and the corresponding envelope spectrum is shown in Fig. 17(b), in which the inner race FCF-related spectral line cannot be recognized, while the rotational frequency harmonics are dominated. Hence, under the interference of strong noise, the Kurtogram cannot work well to select the optimal frequency band for bearing inner race fault diagnosis.

Then, the Protrugram is used to determine the optimal demodulation band and perform envelope spectrum analysis, the results are shown in Fig. 18. The central frequency and the bandwidth of the filtered signal are 5600 Hz and 1600 Hz, respectively, and the target level of the Protrugram is 3, as shown in Fig. 18(a). The corresponding envelope spectrum is displayed in Fig. 18(b), from which we cannot find valuable diagnostic information.

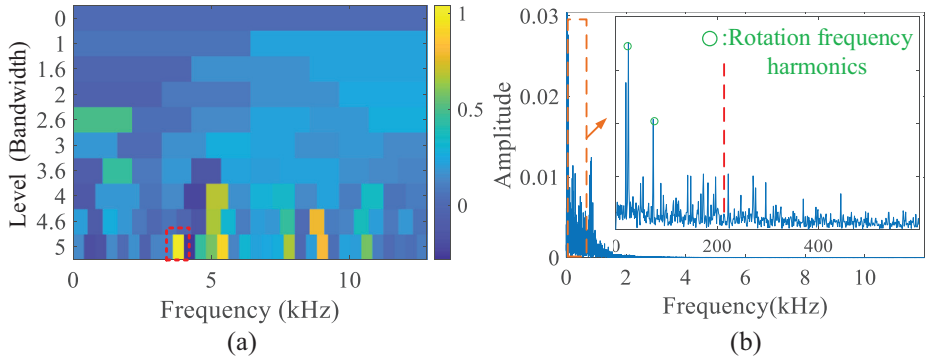

Fig. 17. Analysis results of inner race fault signal using Kurtogram-based method. (a) Kurtogram and (b) Envelope spectrum of the filtered signal.

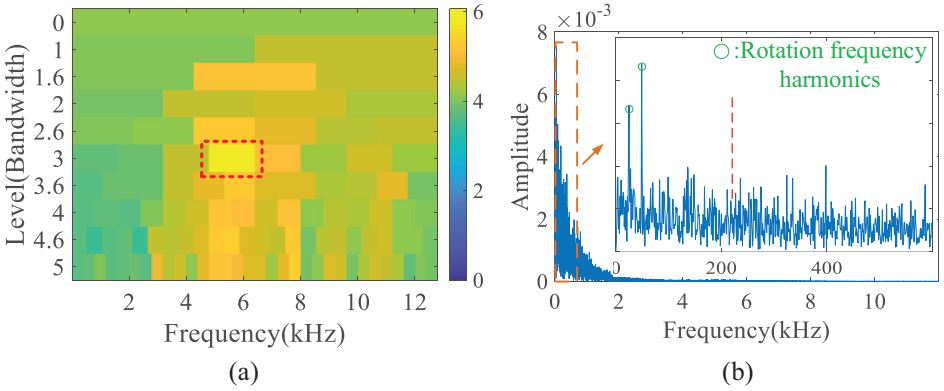

Fig. 18. Analysis results of inner race fault signal using Protrugram-based method. (a) Protrugram and (b) Envelope spectrum of the filtered signal.

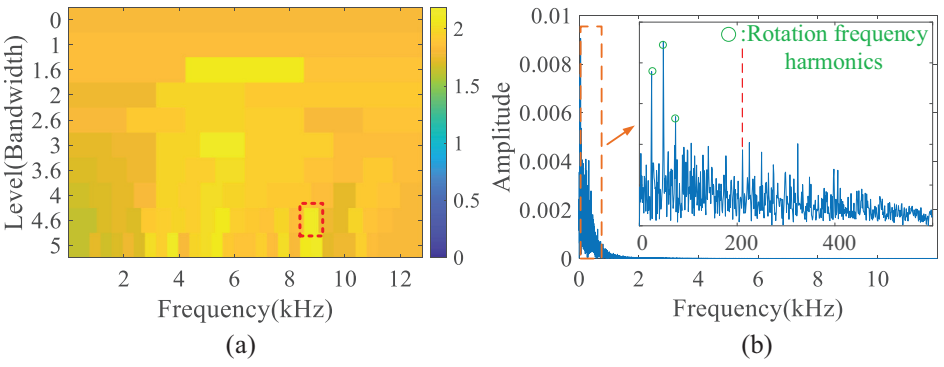

Fig. 19. Analysis results of inner race fault signal using Infogram-based method. (a) Infogram and (b) Envelope spectrum of the filtered signal.

Finally, the SE Infogram is applied to the signal with inner race fault, and the result is displayed in Fig. 19(a). It is clear that the maximum negentropy value is found with a center frequency of 8800 Hz and a bandwidth of 534 Hz. Fig. 19(a) shows the envelope spectrum of the filtered signal, and it can be found that the spectral line related to the FCF of the inner race is buried in strong noise.

In summary, when processing vibration signals of gearbox bearing with inner race fault, the CVgram, Kurtogram, and Protrugram-based methods cannot work well to detect fault characteristics, while the CVRgram can locate the resonance frequency band excited by bearing inner race fault. Hence, the proposed method has a much better ability to detect bearing inner race fault compared with the CVgram, Kurtogram, and Protrugram.

VII. CONCLUSIONS

For addressing the issue that classic parameter index-based filtered methods cannot work well for extracting demodulation bands with low amplitude, a novel index named CVR and CVRgram-based bearing fault diagnosis methods are proposed in this paper. The proposed method is verified by both simulated faulty bearing signal and experiment signal measured from gearbox bearing. Meanwhile, comparison results with Kurtogram, Protrugram, and CVgram are also presented.

(a) The analysis results, related to the simulated signal and experimental signals under strong noise interference, show that the proposed technique can effectively calculate extraction parameters of the resonance frequency band excited by bearing fault, which has relatively weak energy compared with the gear vibration interference, and then, the bearing fault type can be accurately determined.

(b) Comparison results show that the proposed technique has a much better ability for determining the weak demodulation frequency band and detecting bearing fault than the Kurtogram, Protrugram, and CVgram-based methods under strong gear interference.

Moreover, the CVRgram-based fault diagnosis method could be extended for other rotating machinery (e.g., engines and reciprocating machinery) whose vibration signals include strong background interference. Namely, the proposed method can be used to detect the resonance frequency band excited by the mechanical part under strong noise interference.

Acknowledgements

This work is supported by the National Natural Science Foundation of China (Grant Nos. 52075008, 51905292)

CONFLICT OF INTEREST STATEMENT

The authors declare no conflicts of interest.

References

[1] D. Zhao, T. Wang, and F. Chu, "Deep convolutional neural network based planet bearing fault classification," *Comput. Ind.*, vol. 107, pp. 59–66, 2019.

[2] D. Zhao, L. Cui and D. Liu, "Bearing weak fault feature extraction under time-varying speed conditions based on frequency matching demodulation transform," *IEEE/ASME Trans. Mechat.*, 2022.

[3] Y Wang et al., "Spectral kurtosis for fault detection, diagnosis and prognostics of rotating machines: a review with applications," *Mech. Syst. Signal Process.*, vol. 66, pp. 679–698, 2016.

[4] J. Antoni, "The spectral kurtosis: a useful tool for characterising non-stationary signals," *Mech. Syst. Signal Process.*, vol. 20, no. 2, pp. 282–307, 2006.

[5] J. Antoni and R. B. Randall, "The spectral kurtosis: application to the vibratory surveillance and diagnostics of rotating machines," *Mech. Syst. Signal Process.*, vol. 20, no. 2, pp. 308–331, 2006.

[6] J. Antoni, "Fast computation of the kurtogram for the detection of transient faults," *Mech. Syst. Signal Process.*, vol. 21, no. 1, pp. 108–124, 2007.

[7] T. Barszcz and A. JabŁoński, "A novel method for the optimal band selection for vibration signal demodulation and comparison with the Kurtogram," *Mech. Syst. Signal Process.*, vol. 25, no. 1, pp. 431–451, 2011.

[8] A. Moshrefzadeh and A. Fasana, "The Autogram: an effective approach for selecting the optimal demodulation band in rolling element bearings diagnosis," *Mech. Syst. Signal Process.*, vol. 105, pp. 294–318, 2018.

[9] J. Antoni, "The infogram: entropic evidence of the signature of repetitive transients," *Mech. Syst. Signal Process.*, vol. 74, pp. 73–94, 2016.

[10] M. Zhao and J. Lin, "Health assessment of rotating machinery using a rotary encoder," *IEEE Trans. Ind. Electron.*, vol. 65, no. 3, pp. 2548–2556, 2017.

[11] G. Żak et al., "Measures of dependence for-stable distributed processes and its application to diagnostics of local damage in presence of impulsive noise," *Shock Vib.*, vol. 2017, 2017.

[12] J. Hebda-Sobkowicz et al., "Informative frequency band selection in the presence of non-Gaussian noise–a novel approach based on the conditional variance statistic with application to bearing fault diagnosis," *Mech. Syst. Signal Process.*, vol. 145, p. 106971, 2020.

[13] D. Wang, "Some further thoughts about spectral kurtosis, spectral L2/L1 norm, spectral smoothness index and spectral Gini index for characterizing repetitive transients," *Mech. Syst. Signal Process.*, vol. 108, pp. 360–368, 2018.

[14] M. N. Albezzawy, M. G. Nassef, and N. Sawalhi, "Rolling element bearing fault identification using a novel three-step adaptive and automated filtration scheme based on Gini index," *ISA Trans.*, vol. 101, pp. 453–460, 2020.

[15] B. Chen, D. Song, Y. Cheng et al., "IGIgram: An improved Gini index-based envelope analysis for rolling bearing fault diagnosis," *J. Dyn. Monit. Diagn.*, 2022.

[16] A. Mauricio et al., "Improved envelope spectrum via feature optimisation-gram (IESFOgram): a novel tool for rolling element bearing diagnostics under non-stationary operating conditions," *Mech. Syst. Signal Process.*, vol. 144, p. 106891, 2020.

[17] Y. Xu, X. Tang, G. Feng et al., "Orthogonal on-rotor sensing vibrations for condition monitoring of rotating machines," *J. Dyn. Monit. Diagn.*, vol. 1, no. 1, pp. 29–36, 2022.

[18] D. Jelito, and M. Pitera, "New fat-tail normality test based on conditional second moments with applications to finance," *Stat. Papers*, vol. 62, no. 5, pp. 2083–2108, 2021.

[19] P. Jaworski, and M. Pitera, "The 20-60-20 rule," *arXiv preprint arXiv:1501.02513*, pp. 1156–1157, 2015.

[20] D. Liu, L. Cui, and W. Cheng, "Flexible generalized demodulation for intelligent bearing fault diagnosis under nonstationary conditions," *IEEE Trans. Indus. Info.*, 2022.

[21] J. Antoni, "Cyclic spectral analysis of rolling-element bearing signals: facts and fictions," *J. Sound Vib.*, vol. 304, no. 3–5, pp. 497–529, 2007.

[22] T. Wang et al., "Compound faults detection in gearbox via meshing resonance and spectral kurtosis methods," *J. Sound Vib.*, vol. 392, pp. 367–381, 2017.

[23] D. Zhao, J. Li, W. Cheng, et al. Bearing multi-fault diagnosis with iterative generalized demodulation guided by enhanced rotational frequency matching under time-varying speed conditions. ISA transactions, 2022